Short-range spin correlations in β''-$LiFeO_2$ from bulk magnetization, neutron diffraction, and μSR experiments

Ryota Akiyama,[1] Yutaka Ikedo,[2,*] Martin Månsson,[3] Tatsuo Goko,[4] Jun Sugiyama,[2] Daniel Andreica,[5] Alex Amato,[6] Kittiwit Matan,[1] and Taku J. Sato[1,†]

[1]*Neutron Science Laboratory, Institute for Solid State Physics, University of Tokyo, 106-1 Shirakata, Tokai, Ibaraki 319-1106, Japan*

[2]*Toyota Central Research and Development Laboratories Inc., Nagakute, Aichi 480-1192, Japan*

[3]*Laboratory for Neutron Scattering, ETH Zürich and Paul Scherrer Institut, CH-5232 Villigen PSI, Switzerland*

[4]*TRIUMF, 4004 Wesbrook Mall, Vancouver, British Columbia, Canada V6T 2A3*

[5]*Faculty of Physics, Babes-Bolyai University, 3400 Cluj-Napoca, Romania*

[6]*Laboratory for Muon Spin Spectroscopy, Paul Scherrer Institut, CH-5232 Villigen PSI, Switzerland*

(Received 4 October 2009; revised manuscript received 4 December 2009; published 11 January 2010)

Bulk magnetization, neutron-diffraction, and muon-spin-rotation/relaxation (μ^+SR) measurements have been performed to study magnetic ordering behavior in β''-$LiFeO_2$. At room temperature, structural short-range order of Fe atoms was observed with correlation length roughly corresponding to inter-Fe distance. Bulk magnetization, μ^+SR and neutron diffraction all suggest that β''-$LiFeO_2$ is similar to a superparamagnet in the range $110 < T < 170$ K, possibly due to the formation of small spin clusters attributable to atomic short-range order. At lower temperatures, gradual increase in the muon precession frequency as well as the neutron diffuse scattering intensity were observed below 110 K, indicating development of intercluster correlations. While a bulk magnetic ordering was detected in the μ^+SR results, neutron diffraction concludes that the intercluster correlations are definitely short ranged; the correlation length was estimated as $\xi_s \approx 14$ Å, which is almost temperature independent.

DOI: 10.1103/PhysRevB.81.024404 PACS number(s): 76.75.+i, 75.25.−j, 75.50.Ee, 75.50.Lk

I. INTRODUCTION

Lithium transition-metal dioxides ($LiMO_2$ with M=V, Cr, Co, and Ni), belong to the rhombohedral system (space group $R\bar{3}m$) with a layered α-$NaFeO_2$ structure. These compounds have been heavily investigated since 1970s,[1,2] originally due to their complex magnetic nature caused by the layered structure. The structure is formed by an alternating stacking of Li planes in between MO_2 planes in which M ions form a two-dimensional triangular lattice by the connection of edge-sharing MO_6 octahedra. In 1980, it was found that Li ions are easily deintercalated by electrochemical reaction down to $x \approx 0.1$ for $LiMO_2$ with M=Co; in fact, this is the principle behind the operation of Li-ion batteries.[3] Since then, the majority of research into $LiMO_2$ has focused primarily on their electrochemical properties, with the aim of improving $LiCoO_2$ and/or searching for new materials for Li-ion batteries.[4,5] In order to further develop a cheap, safe, and environmentally friendly battery, the most preferable material was naturally thought to be $LiMO_2$ with M=Fe. Unfortunately, a reversible Li intercalation/deintercalation behavior has never been found for $LiFeO_2$ with the α-$NaFeO_2$ structure, probably due to the presence of Fe ions in the Li plane.[6,7]

We have previously initiated a positive muon-spin rotation and relaxation (μ^+SR) investigation of $LiCoO_2$,[8–10] $LiNiO_2$,[11] and $LiCrO_2$ (Ref. 12) to study magnetic ground-state effects due to geometrical frustration in the two-dimensional triangular lattice of the MO_2 plane. Since μ^+SR is very sensitive to local magnetic environments, it is a powerful tool for detecting the short-range magnetic order that often appears for frustrated systems. Indeed, we found the appearance of antiferromagnetic (AF) order for $LiCoO_2$,[8] in contrast to the result of past photoelectron spectroscopic measurements[13] and the prediction from electron structural calculations.[14] For $LiNiO_2$, the ground state was not clarified, in spite of a huge number of magnetic studies[15] including μ^+SR and neutron-scattering measurements.[16,17] Our systematic μ^+SR experiment on Li_xNiO_2 with $0.1 \leq x \leq 1$, however, demonstrated the formation of short-range A-type AF order for $LiNiO_2$ below its T_N(=15 K).[11] Finally, a very recent μ^+SR work on $LiCrO_2$ clearly excluded the formation of short-range magnetic order above T_N(=61.2 K) (Ref. 12) while heat-capacity measurements indicated the presence of a magnetic contribution up to 200 K.[18] It was, therefore, a natural step to extend the investigation into $LiFeO_2$.

Past work on $LiFeO_2$ showed the existence of many structural polymorphs.[6,7,19–25] Even for the compounds containing FeO_6 octahedra, there are eight different phases, that is, cation-disordered α-$LiFeO_2$, cation-ordered tetragonal γ-$LiFeO_2$, and three intermediate phases between them, i.e., β^*-, β'-, and β''-$LiFeO_2$, layered α-$NaFeO_2$-type $LiFeO_2$, layered $LiMnO_2$-type $LiFeO_2$, and hollandite-type $LiFeO_2$. Among them, the β''-$LiFeO_2$ is of particular interest since its structure (illustrated in Fig. 1) is very close to the simple-cubic α phase, where the $(Li,Fe)O_6$ octahedra form three-dimensional cubic lattice. (Indeed, the lattice-constant ratio $c/a \approx 1.01$ in β''-$LiFeO_2$.) It is very interesting to study the effect of magnetic ions at the Li site on the whole magnetic nature of $LiMO_2$, as the Ni ions at the Li site are known to induce a drastic change in the magnetism of $LiNiO_2$.[26] Because of the cation disorder, β''-$LiFeO_2$ is, therefore, thought to be a good reference to clarify such effect. In fact, despite its rather simple structure, β''-$LiFeO_2$ shows quite complicated magnetic behavior as follows: magnetic-susceptibility (χ) and Mössbauer spectroscopy measurements were per-

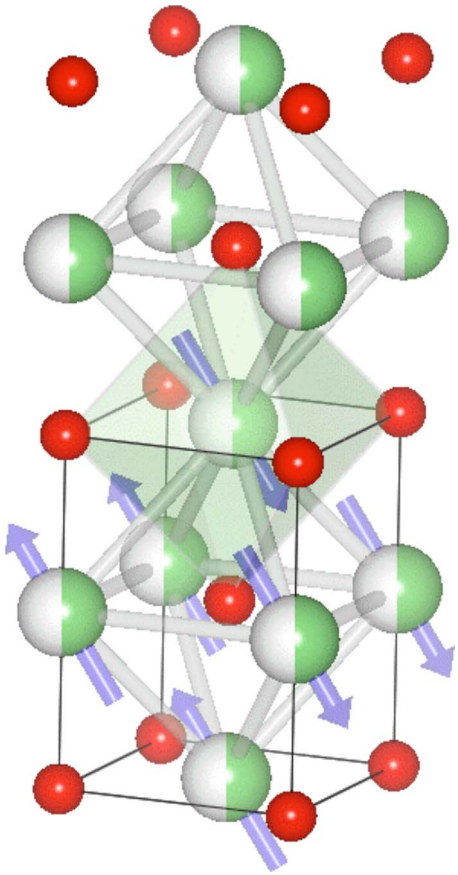

FIG. 1. (Color online) Crystal structure of β''-$LiFeO_2$. Two unit cells are illustrated. The small (red) and big (green/white) spheres denote oxygen and Li/Fe sites, respectively. The thick bars denote an octahedron formed by the Li/Fe atoms, whereas the semitransparent (green) octahedron denotes a $(Li,Fe)O_6$ unit. The (blue) arrows indicate the spin structure of the α-$LiFeO_2$.

formed for the β'' phase by Tabuchi *et al.*[27] The $\chi(T)$ curve obtained in zero-field-cooled (ZFC) mode with a relatively high magnetic field of $H_{ext}=5$ kOe showed two anomalies: at $T_{m1}\approx 120$ K an inflection point is seen, whereas an apparent peak was observed at $T_{m2}\approx 50$ K. The Mössbauer spectrum obtained at the lowest T measured (4.2 K) exhibits clear sextets. Since the sextets were also observed at 77 K, the authors speculated that the magnetic order is established at T_{m1}. This speculation naturally leads to the following questions for the magnetism of β''-$LiFeO_2$: (1) Does the whole volume exhibit the magnetic transition at T_{m1}? (2) Is the magnetic order short range or long range? (3) What is the origin of the anomaly at T_{m2}? (4) What is the ordered spin structure? Since we could not find any systematic study of the magnetic properties of the β''-$LiFeO_2$ in the literature, we have performed both μ^+SR and neutron-diffraction (ND) experiments, together with precise χ measurements with various H_{ext}.

A simple consideration based on the crystal structure of β''-$LiFeO_2$ predicts the absence of long-range magnetic order due to a random distribution of Li and Fe. μ^+SR is, thus, one of the most suitable techniques for investigating the internal magnetic field below T_{m1}. On the other hand, ND provides information on a correlation length of magnetic/atomic order, whether it is short ranged or long ranged while μ^+SR gives no information on the correlation length. Furthermore, since the combination of χ, μ^+SR, and ND measurements covers a wide range of time window and spatial resolution, we can expect to elucidate the complete magnetic nature of β''-$LiFeO_2$.

II. EXPERIMENTAL DETAILS

Powder samples of β''-$LiFeO_2$ were prepared following the method described in Ref. 27: the sample was synthesized using a steam pressure autoclave (98 ml, MR98 OM LABTECH) equipped with a Teflon inner lining to prevent the strong alkali solution to react with the autoclave. We note that there are several confusing notations about the β phases of $LiFeO_2$.[19–21,28] The presently prepared phase is the one defined as the β'' phase in Ref. 27, which indeed is the cation-disordered tetragonal phase with lattice constants $a=2.936$ Å and $c=4.192$ Å. The quality of the prepared sample was checked using powder x-ray diffraction (Cu $K\alpha$), and the ratio of Fe and Li ions was determined to be $Fe/Li=1.074(8)$ using inductively coupled plasma (ICP) mass spectroscopy. Magnetization was measured using a superconducting quantum interference device magnetometer MPMS-XL (Quantum design) in the temperature range $1.8<T<300$ K under several dc external fields.

Muon-spin rotation and relaxation (μ^+SR) spectra were measured at the Swiss Muon Source (SμS), Paul Scherrer Institut, Villigen, Switzerland. By using the surface muon beamline μE1 and the Dolly spectrometer, zero-field (ZF) and weak transverse-field (wTF) spectra were collected for $1.7\ \text{K}\leq T\leq 250$ K. The experimental setup and techniques were described in detail elsewhere.[29] The powder sample was placed in a small envelope made of very thin Al-coated Mylar tape and then attached to a low-background fork-type sample holder.

Neutron-diffraction experiments were performed using the triple-axis spectrometer ISSP-4G GPTAS at the JRR-3 research reactor (Tokai, Japan), operated in double-axis mode. Incident neutrons of $\lambda=1.64$ Å were selected using the pyrolytic graphite (PG) 002 reflections, whereas higher harmonic neutrons were eliminated using the PG filter. Typically, collimations of $40'-20'-20'$ were employed. The powder sample was loaded in a double cylindrical annular sample cell with the outer diameter $\phi_o=22$ mm, inner diameter $\phi_i=19.5$ mm, and height $h=45$ mm. The annular cell was loaded in an Al can and then attached to a closed cycle ^{4}He refrigerator with the lowest working temperature of ≈ 2.4 K.

III. EXPERIMENTAL RESULTS

A. χ measurements

Temperature dependence of field-cooled (FC) and ZFC magnetizations is shown in Fig. 2, measured under several external magnetic fields ranging from $H_{ext}=30$ Oe to 30 kOe. At the lower fields, a bifurcation of the FC and ZFC magnetizations appears around $T_{m0}\approx 170$ K. The bifur-

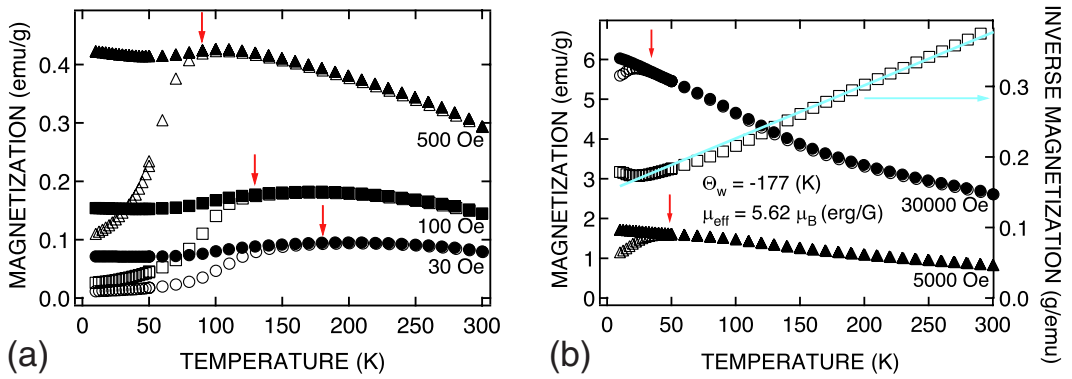

FIG. 2. (Color online) (a) Temperature dependence of FC (closed symbols) and ZFC (open symbols) magnetizations (M) measured under the external magnetic fields H_{ext}=30, 100, and 500 Oe. (b) Temperature dependence of the FC and ZFC magnetizations at higher magnetic fields H_{ext}=5000 and 30 000 Oe. Inverse magnetization ($1/M$) for the ZFC measurement at H_{ext}=30 kOe is also shown. Solid (cyan) line represents results of the inverse Curie-Weiss fit in the temperature range of $150<T<300$ K. In both panels, vertical (red) arrows indicate bifurcation temperatures of the FC and ZFC magnetizations.

cation temperature decreases as the external field increases and it becomes approximately 30 K at the highest field H_{ext}=30 kOe. In an earlier report,[27] an anomaly related to a magnetic ordering is suggested at $T\approx 50$ K from an apparent peak observed in the ZFC susceptibility under H_{ext}=5 kOe. However, as is clearly seen in Fig. 2, the peak temperature in the ZFC run is strongly field dependent, i.e., the assignment of a magnetic anomaly at $T\approx 50$ K in the earlier report is only valid at the specific external field H_{ext}=5 kOe. Therefore, the anomaly at $T\approx 50$ K is not an intrinsic zero-field property but should be regarded as a bifurcation of the same origin as that at T_{m0} under zero field, suppressed continuously to lower temperature by the external field.

The inverse of the ZFC magnetization at H_{ext}=30 kOe is also shown in Fig. 2(b). Linear behavior is clearly seen for the inverse magnetization above 150 K and by fitting the inverse magnetization to the Curie-Weiss law $1/M(T)=(T-\Theta)/CH_{ext}$, we obtained a Weiss temperature $\Theta=-177\pm 1.2$ K and an effective moment size $\mu_{eff}=5.62\pm 0.01\mu_B$. It may be noteworthy that the obtained parameters are only valid for the data taken at H_{ext}=30 kOe; different external field may give different parameters since the field dependence of the magnetization is strongly nonlinear. We note that the size of the presently estimated effective moment is fairly consistent with the one reported by Anderson *et al.*[30] ($\mu_{eff}=5.48\mu_B$) but somewhat deviates from the one by Tabuchi *et al.*[27] ($\mu_{eff}=4.80\pm 0.02\mu_B$). Tabuchi *et al.*[27] infer that their sample includes small amount of an impurity phase ($LiFe_5O_8$) and shows slight deviation in occupation factors from stoichiometry. Thus, we conclude that these two facts are the sources of inconsistency between present μ_{eff} and the one by Tabuchi *et al.*

B. μ^+SR results

The μ^+SR technique provides information regarding the local magnetic environment around μ^+'s, which usually locate in the vicinity of O^{2-} ions, so as to make a stable μ^+-O bond in the β''-$LiFeO_2$ lattice. This is a common situation in oxides, as, for example, in the high-T_c cuprates case[31] or quasi-one-dimensional vanadium oxides.[32]

In order to discover the overall nature of the AF transition, we measured μ^+SR spectra in a wTF (=30 Oe). Here, "weak" means that the applied field is significantly less than any possible spontaneous internal fields (H_{int}) in the ordered state. A wTF-μ^+SR technique is sensitive to local magnetic order via the shift of the μ^+ spin precession frequency and the enhanced μ^+ spin relaxation. Figure 3 shows the variation in the wTF time spectra at different temperatures. When T decreases below $\approx$120 K, the oscillation amplitude due to wTF rapidly decreases, indicating the appearance of additional strong H_{int}. The wTF-μ^+SR spectrum was consequently fitted using a combination of a slowly relaxing precessing signal and an exponentially relaxing nonoscillatory signal. The first component is due to the externally applied magnetic field (wTF=30 Oe) and the second due to H_{int},

$$A_0P_{TF}(t)=A_{TF}\cos(\omega_{TF}^{\mu}t+\phi_{TF})\exp(-\lambda_{TF}t)+A_e\exp(-\lambda_e t), \quad (1)$$

where A_0 is the initial (t=0) asymmetry, $P_{TF}(t)$ is the muon spin-polarization function, ω_{TF}^{μ} is the muon Larmor fre-

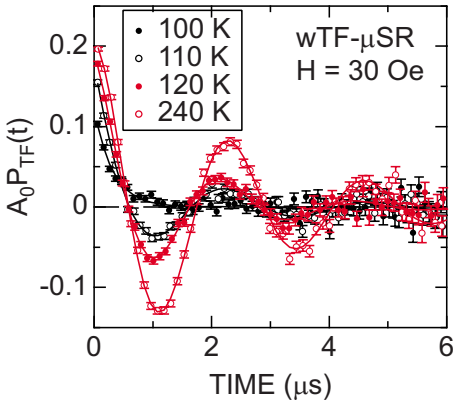

FIG. 3. (Color online) Temperature dependence of the weak transverse-field (wTF=30 Oe)μ^+SR time spectra. Solid lines represent the fitting result using Eq. (1).

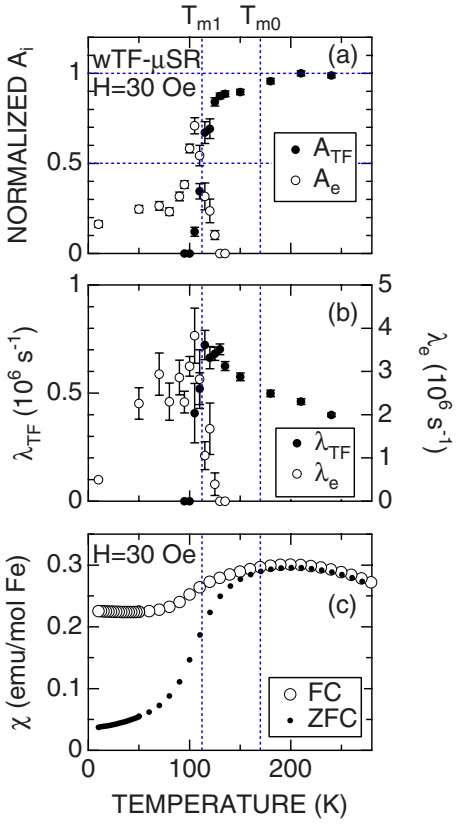

FIG. 4. (Color online) Temperature dependences of (a) normalized asymmetries (A_{TF} and A_e), (b) exponential relaxation rates (λ_{TF} and λ_e), and (c) χ for β''-$LiFeO_2$. The data in (a) and (b) were obtained by fitting the wTF spectra using Eq. (1). χ was measured both in FC and ZFC modes with $H=30$ Oe.

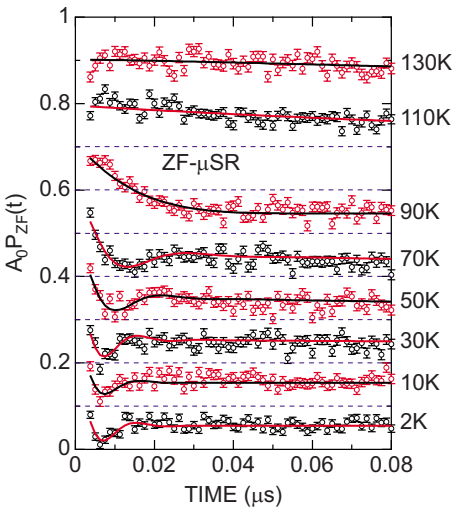

FIG. 5. (Color online) Temperature dependent ZF-μ^+SR spectra for β''-$LiFeO_2$. Solid lines represent the fitting result using Eq. (2). Each spectrum is offset by 0.1 for clarity of display.

quency corresponding to the applied wTF, ϕ_{TF} is the initial phase of the precessing signal, λ_{TF} and λ_e are the exponential relaxation rates, and A_{TF} and A_e are the asymmetries of the two components of the μ^+SR spectrum. This form was chosen because the externally applied magnetic field is much weaker than the local (internal) magnetic fields in the ordered phase. By plotting A_{TF} versus T [see Fig. 4(a)], we can clearly see that the sample has a bulk magnetic transition at $T_{m1}=112.3$ K, where the normalized $A_{TF}(=A_{TF}/A_0=N_{A_{TF}})=0.5$. This is because the normalized A_{TF} corresponds to the volume fraction of paramagnetic (PM) phases in a sample. We wish to emphasize that μ^+SR provides a very clear evidence for the bulk magnetic transition due to its characteristic spatial and time resolution. It may also be noteworthy that the bulk transition takes place at a temperature lower than the freezing temperature T_{m0} detected in the magnetization measurement [see Fig. 2(a)]. This clearly indicates that at T_{m0} only a small portion of the moments freezes; majority of moments remain fluctuating even below the freezing temperature, and order at T_{m1}. Actually, as T decreases from 250 K, $N_{A_{TF}}$ starts to decrease gradually below around T_{m0} and then, suddenly drops down to 0 at T_{m1}.

Although $N_{A_{TF}} \geq 0.9$ above T_{m1}, indicating that almost the whole volume of the $LiFeO_2$ sample is in a paramagnetic state, the $\lambda_{TF}(T)$ curve exhibits a slow increase with decreasing T until T_{m1} is reached. This also indicates an evolution of local magnetic inhomogeneity starting at higher temperature than T_{m1}. On the other hand, since the A_{TF} signal eventually disappears below T_{m1}, it is very difficult to accurately estimate λ_{TF} below T_{m1}. The normalized $A_e(=A_e/A_0=N_{A_e})$ has a nonzero value below T_{m1} and increases with decreasing T down to 105 K, then decreases with further decreasing T, and finally levels off to ≈ 0.3 below 80 K. The fact that N_{A_e} never reaches full asymmetry (=1) suggests the presence of a fast relaxing/precessing signal in the wTF spectrum. However, in order to distinguish such a signal, the ZF-μ^+SR technique with high statistics is more suitable.

In order to demonstrate the magnetic nature below T_{m1}, Fig. 5 shows the T dependence of ZF-μ^+SR time spectra in the T range between 2 and 130 K. Below T_{m1}, a clear first minimum is observed in the ZF-μ^+SR spectrum; the location of the minimum ranges from ≈ 0.007 μs at 2 K to ≈ 0.05 μs at 90 K. The ZF spectrum is so strongly damped that one can be sure that even below T_{m1} *the Fe moments freeze in a highly disordered fashion*, as in the case for Ni moments in $LiNiO_2$.[11] We, thus, attempted to fit the ZF spectrum using a dynamic Gaussian Kubo-Toyabe function $[G^{DGKT}(t,\Delta,\nu)]$ for a fluctuating disordered phase. However, we needed an additional fast relaxing nonoscillatory signal for explaining the rapid decay in the early time domain (below 0.005 μs) of the ZF spectrum. Therefore, the ZF spectrum was fitted by the combination of a damped cosine oscillation, originating from the static ordered H_{int}, and a slowly relaxing nonoscillatory signal due to the "1/3 tail" caused by the field component parallel to the initial muon-spin polarization,

$$A_0 P_{ZF}(t) = A_M \cos(\omega_M^\mu t + \phi_M)\exp(-\lambda_M t) + A_{tail}\exp(-\lambda_{tail} t). \quad (2)$$

Here, A_0 is the initial ($t=0$) asymmetry, $P_{ZF}(t)$ is the muon-spin-polarization function in ZF, $\omega_M^\mu = 2\pi \cdot f_M$ is the muon Larmor frequency corresponding to the ordered H_{int}, ϕ_M is the initial phase of the precessing signal, λ_M is the exponen-

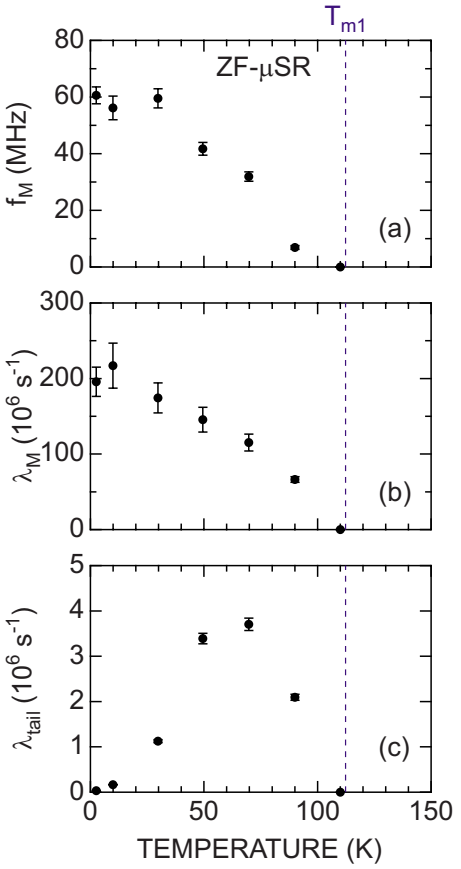

FIG. 6. (Color online) Temperature dependences of (a) muon precession frequency $f_M(=\omega_M^\mu/2\pi)$, (b) exponential relaxation rates (λ_M), and (c) λ_{tail}. The data were obtained by *global* fitting of all the ZF spectra using Eq. (2), with common $A_M(=0.1553\pm0.0003)$, $A_{tail}(=0.0547)$, and $\phi_M=0$.

tial relaxation rate of the precessing signal, λ_{tail} is the exponential relaxation rate of the tail signal, and A_M and A_{tail} are the asymmetries of the two signals.

The fit for the ZF spectrum at the lowest T measured (2.5 K) yields $\phi_M=-9°\pm7°$ (eventually 0), indicating that the spin structure is commensurate to the lattice. This is because incommensurate (IC) magnetic order usually generates broad field distributions at each crystallographic muon site. In fact, the lattice sum calculation of the dipole field at the muon site ($\boldsymbol{H}_{IC}$) due to an IC magnetic structure lies in a plane and traces out an ellipse. The half length of the major axis of the ellipse corresponds to H_{max}, whereas half of the minor axis corresponds to H_{min}. As a result, the IC magnetic field distribution F_{IC} is generally given by[29,33]

$$F_{IC}=F(\boldsymbol{H}_{IC})=\frac{2}{\pi}\frac{H}{\sqrt{(H^2-H_{min}^2)(H_{max}^2-H^2)}}. \quad (3)$$

If we fit the ZF-μ^+SR spectrum produced by F_{IC} using Eq. (2), numerical calculations show that $\phi_M=-45°$,[29] whereas $\phi_M=0°$ for commensurate order. This situation also applies to a powder sample because the muon-spin precesses only by the perpendicular component of H_{int} to the initial muon-spin polarization.

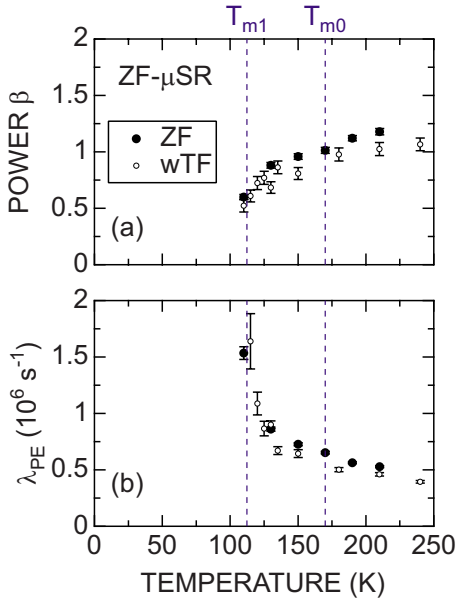

FIG. 7. (Color online) Temperature dependences of (a) β and (b) λ_{PE} for the $LiFeO_2$ powder, particularly above T_{m1}. The ZF data were obtained by fitting using Eq. (4), whereas the wTF data using $A_{TF}\cos(\omega_{TF}^\mu t+\phi_{TF})\exp[-(\lambda_{PE}t)^\beta]$.

Since the preliminary fit at each T indicated that A_M, A_{tail}, and ϕ were almost T independent except below the vicinity of T_{m1}, we attempted to fit all the ZF spectra below T_{m1} using common A_M, A_{tail}, and $\phi=0$, i.e., a *global fit* technique.

Figure 6 shows the T dependences of the μ^+SR parameters obtained by such global fit with common $A_M=0.1553\pm0.0003$ and $A_{tail}=0.0547$. Note that we fixed the total asymmetry at 0.21, i.e., $A_M+A_{tail}=0.21$, based on the wTF-μ^+SR measurements above T_{m1}. Here A_{tail} is approximately comparable to the expected value for the tail ($0.07=0.21/3$). Actually, making comparison with the result of the wTF measurements, A_{tail} is almost equivalent to A_e, which should correspond to the 1/3 tail. This clearly supports the above assignment for the A_{tail} signal.

The $f_M(T)$ curve [Fig. 6(a)] exhibits an order-parameterlike T dependence. That is, as T decreases from T_{m1}, f_M increases monotonically down to ≈30 K, and then appears to level off at a value ≈60 MHz down to the lowest T measured. This behavior is roughly consistent with the neutron result [shown later in Fig. 10(c)], where development of short-range spin correlations was observed. Hence, in the T range between 30 K and T_{m1}, static but highly disordered (or short ranged) Fe moments evolve with decreasing T, and finally, the evolution completes below ≈30 K.

The relaxation rate λ_M also increases monotonically with decreasing T. Although the $\lambda_{tail}(T)$ curve exhibits a maximum around 60 K, its value is two orders of magnitude smaller than λ_M. Furthermore, λ_{tail} approaches 0, when $T\rightarrow0$. But, at high T, λ_{tail} usually has a finite value due to thermal fluctuation of H_{int}.[12,29] Therefore, it is very reasonable to assign this signal as a 1/3 tail signal. Also, this suggests that the fluctuation is gradually suppressed with decreasing T along with the evolution of the magnetic moment.

In order to study the magnetic behavior above T_{m1}, we carried out ZF-μ^+SR measurements also for 110 K$\leq T$

≤ 220 K. In spite of the absence of an oscillatory signal above T_{m1}, the relaxation rate is found to increase rapidly with decreasing T. Since it is difficult to fit the spectrum using a simple exponential relaxation function $[\exp(-\lambda t)]$ in the whole T range between 110 and 220 K, the ZF-μ^+SR spectrum is fitted by a power exponentially relaxing signal,

$$A_0 P_{ZF}(t) = A_{PE} \exp[-(\lambda_{PE} t)^{\beta}]. \quad (4)$$

Such "a power exponentially relaxing signal" has been observed for many dense-moment disordered magnetic system[34,35] in the paramagnetic state. The fit results are shown in Fig. 7. As T decreases from 220 K, $\beta \approx 1$ (simple exponential) down to 170 K, then β decreases with further lowering T, dropping below $\beta=0.5$ (root exponential for a dilute disordered magnet).[36] This means a gradual increase in the number density of localized magnetic moments, which are detectable within the muon time scale, with decreasing T far above T_{m1}. Accompanying the change in β, λ_{PE} also increases gradually below 170 K with decreasing T, which becomes quite rapid as T approaches to T_{m1}. This indicates a broadening of the distribution of H_{int}. This result is therefore consistent with the scenario that disordered moments appear below $T_{m0} \approx 170$ K and develop with decreasing T, and finally static short-ranged order completes below T_{m1}. We infer that some of such disordered moments may fluctuate slowly enough so that they may be responsible for the bifurcation behavior of the ZFC and FC magnetizations at T_{m0}.

C. Neutron scattering

Two anomalies are detected in the magnetization and μ^+SR measurements. At $T_{m0} \approx 170$ K, a bifurcation in the temperature dependence of the ZFC and FC magnetizations was observed, accompanied by the increase in local disordered moments in ZF-μ^+SR spectrum. In addition, a bulk magnetic transition into a highly disordered state was detected in the μ^+SR measurements at $T_{m1} \approx 112.3$ K. We have, therefore, performed a neutron-scattering experiment to gain further insights into the microscopic spin correlations for the two temperature regions. In contrast to the μ^+SR technique, neutron scattering can detect longer-range spatial correlations for both the spins and atoms.

Neutron powder-diffraction patterns at four temperatures $T=2.4$, 50, 150, and 300 K are shown in Figs. 8(a)–8(d). There are several extrinsic reflections due to the Al sample cell, which are indicated by arrows in the figure. Other reflections are all indexed by those of the β''-$LiFeO_2$ structure, confirming absence of contamination phases in the present sample. The crystallographic parameters were obtained by performing Rietveld analysis using the General Structure Analysis System (GSAS) suite[38,39] for the diffraction data in the range of $30° < 2\theta < 90°$. In the Rietveld analysis, the occupation factors for Fe and Li ions are fixed at 0.518 and 0.482, respectively, as determined by the ICP analysis. The optimal lattice parameters at the four temperatures are summarized in Table I and the resulting calculated profiles are also depicted in Fig. 8. Satisfactory correspondences can be seen between the observed and calculated profiles, confirming the validity of the estimated parameters. A larger lattice

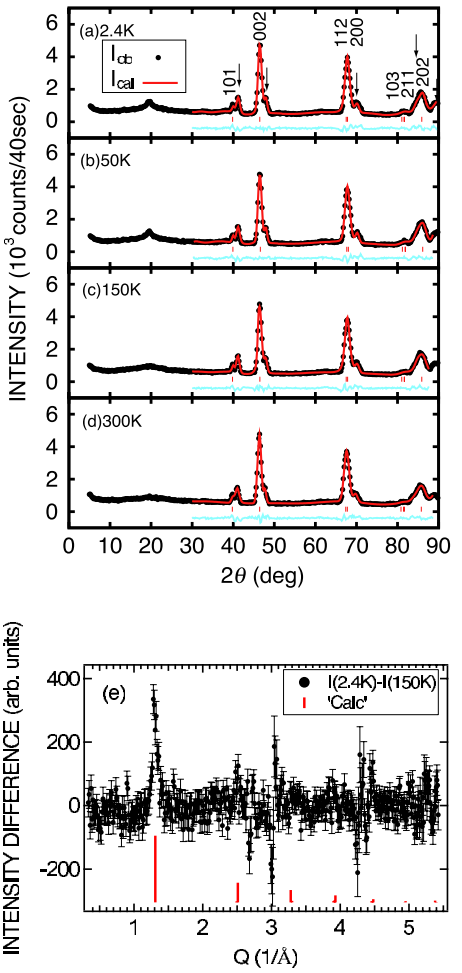

FIG. 8. (Color online) [(a)–(d)] Neutron powder-diffraction patterns of β''-$LiFeO_2$ at $T=2.4$, 50, 150, and 300 K. Reflection indices are given for the pattern at 2.4 K, whereas the vertical arrows stand for powder-diffraction peaks from the aluminum sample cell. Solid (red) lines stand for the results of the Rietveld fitting assuming β''-$LiFeO_2$ structure and the contaminating aluminum reflections. (e) The temperature difference between the $T=2.4$ and 300 K patterns. Vertical solid (red) lines indicate expected magnetic reflection positions assuming the same spin structure as observed in α-$LiFeO_2$ (Ref. 37).

contraction may be seen for the c axis rather than the a axis as the temperature is decreased and the ratio of $\sqrt{2}a/c$ becomes closer to unity at base temperature.

As the temperature is lowered, several extra (magnetic) scattering peaks appear in the diffractogram; with the most

TABLE I. Lattice parameters at the four temperatures $T=2.4$, 50, 150, and 300 K determined using the Rietveld method.

Temperature (K)	a (Å)	c (Å)
300	2.9322(5)	4.1896(12)
150	2.9301(5)	4.1814(11)
50	2.9230(5)	4.1746(12)
2.4	2.9306(7)	4.1797(14)

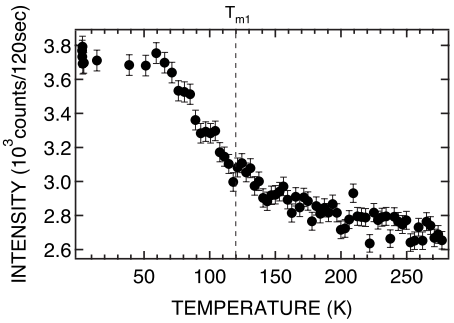

FIG. 9. Temperature dependence of the magnetic peak intensity in β''-$LiFeO_2$ observed at $2\theta=19.5°$.

prominent at around $2\theta=19.5°$. The temperature dependence of the scattering intensity observed at $2\theta=19.5°$ is shown in Fig. 9. The intensity starts to increase gradually below $T \approx 200$ K, which is in rough agreement with T_{m0} detected in the μ^+SR and magnetization measurements, having the difference of times scales in these methods in mind. This confirms the magnetic origin of the increase in the scattering intensity and definitely shows an increase in slowly fluctuating moments in the time window of the neutron experiment (i.e., slower than tetrahertz). As further decreasing temperature, the slope becomes relatively steeper below 120 K. In the later paragraphs [with Fig. 10(c)], we will show that this change in the slope indeed corresponds to development of scattering intensity from short-range spin correlations. This temperature is in good agreement with the temperature where the μ^+SR signal shows bulk magnetic transition (Figs. 4 and 6) and the low-field ZFC susceptibility shows a steep downturn (Fig. 2). The intensity becomes roughly constant below 50 K, indicating that the increase in magnetic moments finishes around this temperature. This behavior is also consistent with the μ^+SR results shown in Fig. 6(a).

To more clearly distinguish the evolution of the magnetic correlations, we have examined peak profiles around the $Q \approx 1.3$ Å^{-1} ($2\theta=19.5°$) in detail. The results are shown in Fig. 10(a). From the observed profiles, one can clearly see that there are two overlapping peaks in this range. One is a relatively sharp peak, observed only at low temperatures ($T=2.4$ and 50 K). The other is the broad component (underneath the sharp peak), which is roughly temperature independent up to 300 K. To parameterize their temperature dependence, the data were fitted to the following function consisting of two Gaussians:

$$I(Q) = \frac{a_1}{\sqrt{2\pi}\sigma_1}\exp\left[-\frac{(Q-b_0)^2}{2\sigma_1^2}\right] + \frac{a_2}{\sqrt{2\pi}\sigma_2}\exp\left[-\frac{(Q-b_0)^2}{2\sigma_2^2}\right] + c_1. \quad (5)$$

Figures 10(b) and 10(c) show the temperature dependence of the obtained width σ_1 (σ_2) parameter (converted into full width at half maximum, FWHM) and intensity parameter $a_1/\sqrt{2}\sigma_1$ ($a_2/\sqrt{2}\sigma_2$), respectively. For the sharp peak, the intensity decreases quickly as temperature is increased. We note that the instrumental resolution estimated using standard Al_2O_3 reflections is $\Delta Q=3\times10^{-2}$ Å^{-1} (FWHM) at $Q \approx 1.3$ Å^{-1}, which is considerably smaller than the peak width. This suggests that the corresponding spin correlations are short ranged even at the lowest temperature. The correlation length was estimated as $\xi_s \approx 14$ Å from the peak width, after correcting for the resolution effect. On the other hand, the broad component shows almost temperature independent width and intensity. This corresponds to the very short correlation of $\xi_b \approx 2$ Å, which is as short as the inter-Fe/Li distance. Since the broad component stays unchanged even at room temperature, it is highly likely it is of structural origin. Related cation short-range order can be found in α-$LiFeO_2$, as reported in an electron-diffraction study.[40]

The difference between the neutron-diffraction patterns at $T=2.4$ and 150 K is shown in Fig. 8(e). Although several magnetic peaks are visible in the difference plot, they are generally weak and broad, and thus the magnetic structure cannot be uniquely determined solely from the diffraction data. In the literature, the magnetic structure of the α-$LiFeO_2$, which has similar cation-disordered crystal structure, was determined using powder neutron diffraction as the A-type AF structure.[37] We, therefore, applied this magnetic structure to the present β''-$LiFeO_2$. The magnetic reflection positions for the A-type AF structure are shown by the vertical solid lines in Fig. 8(e), with their lengths representing the expected powder reflection intensity. As can be seen in the figure, the correspondence between the observed and calculated magnetic peak positions and intensities is satisfactory, indicating that short-range A-type AF order, indicated by the arrows in Fig. 1, may be realized also in β''-$LiFeO_2$.

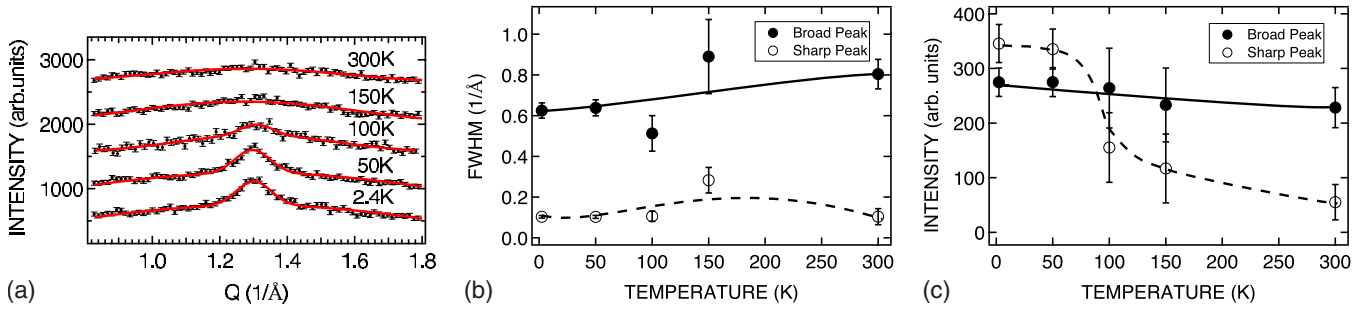

FIG. 10. (Color online) (a) Neutron-diffraction patterns at the four temperatures $T=300$, 150, 50, and 2.4 K in the low 2θ region. Solid (red) lines stand for the fitting results to the model function consisting of two Gaussians. (b) Temperature dependence of the widths (FWHM) of the broad (closed circles) and sharp (open circles) peaks. (c) Temperature dependence of the intensities for the broad (closed circles) and sharp (open circles) peaks. The intensities are estimated by the Gaussian fitting as described in the text.

IV. DISCUSSION

A. Structural short-range order

The broad diffuse scattering observed in the neutron-diffraction pattern at room temperature suggests that there is a short-range cation ordering for the Li and Fe atoms. As postulated by Brunel *et al.*,[41] the charge of the oxygen has to be compensated in the octahedral environment with cation short-range order[42] to satisfy the Pauling's electrostatic valence rule.[43] Therefore, the corners of the tetrahedron (Fig. 1) have to be occupied by three Li^{1+} and three Fe^{3+}. As discussed for the related α-$LiFeO_2$, there are only two types of Fe^{3+} arrangements that satisfy the local charge compensation:[40] one is a linear Fe-atom arrangement along the ridge of the octahedron, whereas the other is a planar ordering of Fe atoms in an 011 plane. (Note that the 011 direction in the tetragonal coordinate corresponds to the 111 direction in the cubic coordinate with which α-$LiFeO_2$ is defined.) In the latter case, the other 011 plane will be occupied by Li atoms, and thus there will be a short-ranged alternating stack of the Li and Fe planes along the 011 direction. This will give rise to the broad diffuse scattering around the $0\frac{1}{2}\frac{1}{2}$ position ($2\theta=19.5°$), which is indeed observed in the experiment.

B. Two-step freezing

Because of the chemical inhomogeneity due to the short-range order of Fe atoms, very small spin clusters with characteristic length scale of ≈ 2 Å are probably first formed with decreasing temperature. The bifurcation in the temperature dependence of the ZFC and FC magnetizations at T_{m0} indicates that freezing of cluster moments takes place for some spin clusters with large spin-flip-energy barrier. On the other hand, the development of the neutron diffuse scattering intensity is quite weak and no oscillatory but only "power exponentially relaxing" signal was observed in the μ^+SR spectra for $T_{m1}<T<T_{m0}$. Therefore, the majority of the spins are still fluctuating and the frozen clusters form small islands in a paramagnetic phase. Hence, we suggest that the anomaly at T_{m0} is rather similar to the blocking of the superparamagnet, where cluster moments freeze due to their own anisotropic barrier, independently of adjacent clusters. It should be noted that because the Fe clusters are sandwiched between the Li clusters as described above, even the ferromagnetic (FM) spin correlations would give rise to the magnetic diffuse scattering intensity around the seemingly AF position $0\frac{1}{2}\frac{1}{2}$. Therefore, we cannot conclude whether the correlation in these very small spin clusters (containing only a few Fe atoms) is FM or AF.

As the temperature is lowered below T_{m1}, the muon-spin precession frequency (f_M) starts to increase, indicating development of internal magnetic fields due to longer-range spin correlations. Concomitantly, neutron diffraction detects sharper diffuse scattering, showing that the spin-correlation length increases to $\xi_s \approx 14$ Å. Since A_{TF} in the TF-μ^+SR disappears, all the spins have static moment, i.e., a finite expectation value for the spin operator $\langle S_i \rangle$ at any ith site, below T_{m1}, although spatially only short-range correlations are established. The diffuse peak appears at $0\frac{1}{2}\frac{1}{2}$, suggesting the AF nature of the intercluster correlations. Since the muon precession frequency f_M and neutron diffuse scattering intensity further increase gradually below T_{m1}, the static moment $\langle S_i \rangle$ grows down to $T \approx 50$ K, where both of them saturates. We wish to emphasize that the spin correlation never reaches infinite and thus the magnetic order is only short ranged even at lowest temperature, although a bulk ordering is established (i.e., all the moments are frozen.) The damped oscillation in the ZF-μ^+SR spectrum even at the lowest T measured, i.e., "Kubo-Toyabe-type" oscillation also supports the above discussion/estimation. We infer that intrinsic randomness due to the chemical disorder may be the origin of short-range order at base temperature.

V. SUMMARY

We have performed complementary magnetization, neutron-diffraction, and μ^+SR measurements to study magnetic ordering behavior in β''-$LiFeO_2$. The neutron powder diffraction at room temperature detects chemical inhomogeneity for the Fe/Li atoms; small Fe-atom clusters with the length scale of $\xi_b \approx 2$ Å are observed. For the magnetic ordering we found a very intriguing two-step freezing behavior. As temperature is decreased, the moment fluctuations first become slower below $T_{m0} \approx 170$ K, with small amount of spin clusters frozen below this temperature. This suggests that β''-$LiFeO_2$ behaves similarly to a superparamagnet, consisting of very small spin clusters formed in the short-range clustering of Fe atoms. At $T_{m1} \approx 110$ K, bulk magnetic order is detected in the μ^+SR measurement, whereas the neutron diffraction only detects finite-spatial-length correlation ($\xi_s \approx 14$ Å) down to the lowest temperature. This indicates that only short-range AF order is established in β''-$LiFeO_2$, most likely due to the intrinsic randomness caused by chemical disorder.

ACKNOWLEDGMENTS

R.A. and T.J.S. would like to thank Zenji Hiroi and Hiroyuki Yoshida at ISSP for permitting us to use their steam pressure autoclave and Yoko Kiuchi for the ICP measurements. This work has been partly performed using the facilities of MDCL, ISSP, University of Tokyo. The μ^+SR experiment was performed at the Swiss Muon Source, Paul Scherrer Institut, Villigen, Switzerland and we are thankful to Robert Scheuermann for assistance with the μ^+SR experiments. Y.I. and J.S. are partially supported by the KEK-MSL InterUniversity Program for Overseas Muon Facilities. This work is also supported by Grant-in-Aid for Scientific Research (B), Grant No. 19340107, MEXT, Japan. All images involving crystal structure were made with VESTA (Ref. 44).

*Present address: Muon Science Laboratory, Institute of Materials Structure Science, KEK, 1-1 Oho, Tsukuba, Ibaraki 305-0801, Japan.
†taku@issp.u-tokyo.ac.jp

[1] T. A. Hewston and B. L. Chamberland, J. Phys. Chem. Solids **48**, 97 (1987).
[2] K. Hirakawa, H. Kadowaki, and K. Ubukoshi, J. Phys. Soc. Jpn. **54**, 3526 (1985).
[3] K. Mizushima, P. C. Jones, P. J. Wiseman, and J. B. Goodenough, Mater. Res. Bull. **15**, 783 (1980).
[4] T. Ohzuku and R. J. Brodd, J. Power Sources **174**, 449 (2007).
[5] L. Sebastian and J. Gopalakrishnan, J. Mater. Chem. **13**, 433 (2003).
[6] T. Shirane, R. Kanno, Y. Kawamoto, Y. Takeda, M. Takano, T. Kamiyama, and F. Izumi, Solid State Ionics **79**, 227 (1995).
[7] K. Ado, M. Tabuchi, H. Kobayashi, H. Kageyama, Y. I. O. Nakamura, R. Kanno, M. Takagi, and Y. Takeda, J. Electrochem. Soc. **144**, L177 (1997).
[8] J. Sugiyama, H. Nozaki, J. H. Brewer, E. J. Ansaldo, G. D. Morris, and C. Delmas, Phys. Rev. B **72**, 144424 (2005).
[9] K. Mukai, Y. Ikedo, H. Nozaki, J. Sugiyama, K. Nishiyama, D. Andreica, A. Amato, P. L. Russo, E. J. Ansaldo, J. H. Brewer, K. H. Chow, K. Ariyoshi, and T. Ohzuku, Phys. Rev. Lett. **99**, 087601 (2007).
[10] J. Sugiyama, K. Mukai, Y. Ikedo, H. Nozaki, M. Månsson, and I. Watanabe, Phys. Rev. Lett. **103**, 147601 (2009).
[11] J. Sugiyama, K. Mukai, Y. Ikedo, P. L. Russo, H. Nozaki, D. Andreica, A. Amato, K. Ariyoshi, and T. Ohzuku, Phys. Rev. B **78**, 144412 (2008).
[12] J. Sugiyama, M. Månsson, Y. Ikedo, T. Goko, K. Mukai, D. Andreica, A. Amato, K. Ariyoshi, and T. Ohzuku, Phys. Rev. B **79**, 184411 (2009).
[13] J. van Elp, J. L. Wieland, H. Eskes, P. Kuiper, G. A. Sawatzky, F. M. F. de Groot, and T. S. Turner, Phys. Rev. B **44**, 6090 (1991).
[14] M. T. Czyżyk, R. Potze, and G. A. Sawatzky, Phys. Rev. B **46**, 3729 (1992).
[15] A. J. W. Reitsma, L. F. Feiner, and A. M. Olés, New J. Phys. **7**, 121 (2005).
[16] T. Chatterji, W. Henggeler, and C. Delmas, J. Phys.: Condens. Matter **17**, 1341 (2005).
[17] J.-H. Chung, T. Proffen, S. Shamoto, A. M. Ghorayeb, L. Croguennec, W. Tian, B. C. Sales, R. Jin, D. Mandrus, and T. Egami, Phys. Rev. B **71**, 064410 (2005).
[18] L. K. Alexander, N. Büttgen, R. Nath, A. V. Mahajan, and A. Loidl, Phys. Rev. B **76**, 064429 (2007).
[19] M. Brunel and F. D. Bergevin, J. Phys. Chem. Solids **29**, 163 (1968).
[20] R. Famery, P. Bassoul, and F. Queyroux, J. Solid State Chem. **57**, 178 (1985).
[21] R. Famery, P. Bassoul, and F. Queyroux, J. Solid State Chem. **61**, 293 (1986).
[22] B. Fuchs and S. Kemmler-Sack, Solid State Ionics **68**, 279 (1994).
[23] R. Kanno, Y. K. T. Shirane, Y. Takeda, M. Takano, M. Ohashi, and Y. Yamaguchi, J. Electrochem. Soc. **143**, 2435 (1996).
[24] Y. Sakurai, H. Arai, S. Okada, and J. Yamaki, J. Power Sources **68**, 711 (1997).
[25] T. Matsumura, R. Kanno, Y. Inabe, Y. Kawamoto, and M. Takano, J. Electrochem. Soc. **149**, A1509 (2002).
[26] J. N. Reimers, J. R. Dahn, J. E. Greedan, C. V. Stager, G. Liu, I. Davidson, and U. V. Sacken, J. Solid State Chem. **102**, 542 (1993).
[27] M. Tabuchi, S. Tsutsui, C. Masquelier, R. Kanno, K. Ado, I. Matsubara, S. Nasu, and H. Kageyama, J. Solid State Chem. **140**, 159 (1998).
[28] M. Tabuchi, K. Ado, H. Sakaebe, C. Masquelier, H. Kageyama, and O. Nakamura, Solid State Ionics **79**, 220 (1995).
[29] G. M. Kalvius, D. R. Noakes, and O. Hartmann, *Handbook on the Physics and Chemistry of Rare Earths* (North-Holland, Amsterdam, 2001), Vol. 32, Chap. 206.
[30] J. C. Anderson, S. K. Dey, and V. Halpern, J. Phys. Chem. Solids **26**, 1555 (1965).
[31] T. R. Adams, R. L. Lichti, and T. L. Gibson, Hyperfine Interact. **86**, 561 (1994).
[32] J. Sugiyama, Y. Ikedo, T. Goko, E. J. Ansaldo, J. H. Brewer, P. L. Russo, K. H. Chow, and H. Sakurai, Phys. Rev. B **78**, 224406 (2008).
[33] D. Andreica, Ph.D. thesis, IPP/ETH-Zurich, 2001.
[34] D. R. Noakes, G. M. Kalvius, R. Wappling, C. E. Stronach, M. F. White, Jr., H. Saito, and K. Fukamichi, Phys. Lett. A **238**, 197 (1998).
[35] D. R. Noakes, G. M. Kalvius, and O. Hartmann, Phys. Rev. B **65**, 132413 (2002).
[36] Y. J. Uemura, T. Yamazaki, R. S. Hayano, R. Nakai, and C. Y. Huang, Phys. Rev. Lett. **45**, 583 (1980).
[37] D. E. Cox, G. Shirane, P. A. Flinn, S. L. Ruby, and W. J. Takei, Phys. Rev. **132**, 1547 (1963).
[38] A. Larson and R. V. Dreele, General Structure Analysis System (GSAS), Los Alamos National Laboratory Report No. LAUR 86-748, 1994 (unpublished).
[39] B. H. Toby, J. Appl. Crystallogr. **34**, 210 (2001).
[40] S. Kohiki, K. Hori, K. Ogawa, H. Shimooka, T. Tajiri, H. Deguchi, M. Mitome, and Y. Bando, Jpn. J. Appl. Phys. **43**, L1232 (2004).
[41] M. Brunel, F. de Bergevin, and M. Gondrand, J. Phys. Chem. Solids **33**, 1927 (1972).
[42] M. Sauvage and E. Parthe, Acta Crystallogr., Sect. A: Cryst. Phys., Diffr., Theor. Gen. Crystallogr. **30**, 239 (1974).
[43] L. Pauling, *The Nature of the Chemical Bond*, 3rd ed. (Cornell University Press, Ithaca, 1960), p. 547.
[44] K. Momma and F. Izumi, J. Appl. Crystallogr. **41**, 653 (2008).